18

Nanoparticle Dynamics in Polymer Melts

Giovanni Filippone and Domenico Acierno
Dept. of Materials and Production Engineering, University of Naples Federico II
Italy

1. Introduction

Adding solid particles to polymeric materials is a common way to reduce the costs and to impart desired mechanical and transport properties. This makes polymers potential substitutes for more expensive non-polymeric materials. The advantages of filled polymers are normally offset by the increased complexity in the rheological behaviour of the resulting composite. Usually, a compromise has to be made between the benefits ensured by the filler, the increased difficulties in melt processing, the problems in achieving a uniform dispersion of the solid particulate, and the economics of the process due to the added step of compounding [Shenoy, 1999]. Filled polymers can be described as a suspension of particles and particle aggregates dispersed in the polymer matrix. Interactions between individual particles or aggregates and the matrix, as well as between particles, hinder the material deformability modifying both the solid- and melt-state behaviour of the host polymer. In polymer-based microcomposites, these effects only become significant at relatively high filler contents, i.e. when the filler particles are sufficiently close to each other to form a network that spans large sections of the polymer matrix. Over the last fifteen years, the same reinforcing and thixotropic effects have been observed with the use of very small amounts of inorganic nanoparticles, which has resulted in extensive research in the field of polymer-based nanocomposites (PNCs) [Usuki et al., 1993; Kojima et al., 1993]. In order to fully understand the exceptional properties of PNCs, the morphological and structural implications stemming from the nanometric sizes of the filler have to be taken into account. With respect to traditional microcomposites, nanocomposites show very high specific interface area, typically of order of ~10^2 m^2 g^{-1}. The matrix properties are significantly affected in the vicinity of the reinforcement, varying continuously from the interface towards the bulk polymer. As a consequence, the large amount of reinforcement surface area means that a relatively small amount of nanoscale reinforcement can have remarkable effects on the macroscale properties of the composite material.

A noticeable consequence of the nanometric dimensions of the filler is the extremely high numerical density of particles, or alternatively the very small inter-particles distances. If N monodisperse spherical particles with radius r are randomly distributed in a volume V, the distance between the centres of the particles can be approximated to $h=(V/N)^{1/3}$. Introducing the particle volume fraction $\Phi=Nv/V$, where $v=4\pi r^3/3$ is the volume of the single particle, the wall-to-wall distance between contiguous particles is:

$$h = \left[\sqrt[3]{\frac{4\pi}{3\Phi}} - 2 \right] r \tag{1}$$

Once fixed the filler content, h linearly scales with r. In addition, we observe that, for diluted systems (Φ<0.1) such those we are interested in, Eq. 1 gives h~2r. This means that, if the filler particles are well dispersed within the host polymer, nanometric inter-particles distances are expected for nanocomposites. In such systems a large fraction of polymer is in contact with the filler. At the most, if the particle radius is of the same order as the mean radius of gyration of host polymer chains, R_g, each single chain potentially interacts with more than one nanoparticle, and there is no bulk polymer [Jancar & Recman, 2010]. Two scenarios are possible when inter-particles distances are so small: if a good affinity exists between the polymer and the filler, then a polymer-mediated transient network between the particles set up [Ozmusul et al., 2005; Saint-Michel et al., 2003; Zhang & Archer, 2002]; on the other hand, if the polymer-filler interactions are weak, the nanoparticles aggregate forming flocs, which eventually assemble into a space-spanning filler network [Filippone et al. 2009; Inoubli et al., 2006; Ren et al., 2000]. In both cases, the presence of a three-dimensional mesostructure has a profound effect on the composite rheology.

The formation of the network, either polymer-mediated or formed by bare nanoparticles, originates from local rearrangements of the filler occurring in the melt both during flow and at rest. Nanoparticles, in fact, are subjected to relevant Brownian motion even in highly viscous mediums such as polymer melts. To get an idea about the relevance of such a phenomenon, we estimate the self-diffusion time of a spherical particle of radius r, τ_s, that is the time required for the particle moves of a length equal to its radius [Russel et al., 1989]:

$$\tau_s = \frac{6\pi\eta_s r^3}{k_B T} \tag{2}$$

Here η_s is the viscosity of the suspending medium, k_B is the Boltzmann's constant and T is the temperature. For a simple low viscosity (η_s~10^{-2} Pa*s) Newtonian liquid at room temperature, Eq. 2 gives the well-known result that particles of a few microns in size experience appreciable Brownian motions. Setting T=400°K and η_s~10^3 Pa*s as typical values for melted polymers, we obtain the noteworthy result that particles of a few tens of nanometers display Brownian motions on timescales of order of a $10^1 \div 10^2$ seconds. Such durations are typically accessed in many transforming processes of the polymer industry, as well as during rheological analyses. The result is that, unlike polymer microcomposites, PNCs can be depicted as "living systems", in which the particles are free to move and rearrange in the melt, both in flow and even at rest, towards more favourable thermodynamic states. In this sense, PNCs are reminiscent of colloidal suspensions. Therefore, these simpler systems can be considered as the natural starting point to understand the much more complex rheological behaviour of PNCs.

The simplest case of colloidal dispersion is represented by a Newtonian suspension of hard spheres. The inter-particles interaction is zero at all separations and infinitely repulsive at contact. Coupled with thermal fluctuations, this kind of interaction results in a wide variety of possible structures. The suspension may behave like a gas, a liquid, a crystal or a glass depending on the particle volume fraction Φ [Pusey & van Megen, 1986]. In the presence of

interactions, this phase behaviour is modified due to interplay between Φ and the energy of interaction, U. We are mainly interested in weakly attractive colloidal dispersions, which are reminiscent of a large number of PNCs in which Van der Waals forces between nanoparticles and aggregates are of major importance. In such systems, aggregation results in disordered clusters of particles. These mesostructures may or may not span the whole space depending on Φ and U [Prasad, 2003]. The rheological behaviour of weakly interacting colloidal dispersions can be rationalized with a simple two-phase model that combines the elasticity of the disordered particle network and the Newtonian viscosity of the suspending liquid [Cipelletti et al., 2000; Trappe & Weitz, 2000; Trappe et al., 2001]. Despite the complexities stemming from the intrinsic non-Newtonian feature of polymer matrices, in this chapter we show that a similar approach can be successfully applied to a series of model PNCs with weak polymer-filler interaction. We emphasize that many PNCs of technological interest fall in this family. The two-phase model is validated through the building of a master curve of the elastic modulus of samples at different composition. A refinement of the model is also presented, which accounts for hydrodynamic effects. The dynamics of de-structuring and reforming of the filler network are studied by analysing the effects of large amplitude deformations. Besides simplifying the viscoelastic analysis of complex systems such as PNCs, the proposed approach can be extended to a wide variety of complex fluids where the elasticity of the components can be superimposed. In particular, the elastic modulus has been recently suggested to follow a universal behaviour with volume fraction also in case of interacting systems in which polymer bridging mechanisms exist [Surve et al., 2006]. This suggests a possible general feature for the proposed approach.

2. Viscoelasticity and structure of PNCs

We start our analysis dealing with the implications of Brownian motion in simple model systems constituted by polymer melts filled with small amounts of different kinds of spherical particles. Specifically, we discuss the effect of particle size and matrix viscosity on the ability of the filler to aggregate and eventually assemble in a three-dimensional network. Then, a two-phase model firstly proposed for weakly attractive particles suspended in a Newtonian medium is presented [Trappe & Weitz, 2000]. The physical picture of an elastic particle network interspersed in a background fluid qualitatively accounts for the viscoelastic behaviour of the suspension. Afterwards, the relations between structure and viscoelasticity of two model PNCs is described in the framework of the two-phase model. A refinement of the model is therefore presented, which accounts for hydrodynamic effects successfully capturing the frequency dependent viscoelastic behaviour of simple PNCs. Finally, the dynamics of de-structuring and reforming of the filler network are studied by analysing the effects of large amplitude deformations.

2.1 Brownian motion in polymer melts filled with nanoparticles – Gelation and ageing

2.1.1 Preliminary considerations

Untreated inorganic particles are difficult to disperse in polymer matrices due to the typically poor polymer-filler affinity. Such incompatibility clearly emerges in the case of PNCs, where the specific surface of the particles is very high. The hydrodynamic forces

developed during intense melt mixing processes breakup the large aggregates down to clusters of few tens of particles [Baird & Collias, 1998]. Above the melting or glass transition temperature of the polymer matrix, however, these aggregates may reassemble into bigger structures because of the inter-particles attraction forces. Since the refractive indexes of polymers and inorganic fillers are typically very different, Van der Waals forces becomes of major importance leading to formation of aggregates and particle gels. The two most simple experimental techniques to follow the rearrangements of the filler in the melt are: (i) direct visualization of the particles through electron microscopy performed on solid samples; (ii) monitoring of rheological parameters sensitive to the material internal structure. Both these techniques have been applied to several model PNC systems constituted by polymer matrices filled with different kinds of inorganic nanoparticles with spherical symmetry. The rational for selecting such model systems originates from the intrinsic high complexity of other technologically relevant PNCs. The properties of such systems, often based on layered or tubular nanoparticles, are too sensitive to the state of dispersion of the filler and the wide variety of the possible nanostructures achievable during processing. The materials, the compounding procedures and the experimental details about the characterization of the composites are described in detail in the following paragraphs. Many of the results have been taken from papers previously published by our group, wherein further experimental details can be found [Acierno et al., 2007a, 2007b; Romeo et al., 2008; Filippone et al., 2010; Romeo et al., 2009].

2.1.2 Materials and sample preparation

Nano- and microcomposites were prepared using two different polymeric matrices. The first one is polypropylene (PP Moplen HP563N by Basell; weight average molecular weight M_w=245 KDa; zero shear viscosity η_0=1.9*10^3 Pa*s at 190°C; terminal relaxation time τ_t≈0.4 s) with glass transition temperature T_g=6°C and melting temperature T_m=169°C. The second polymer matrix is atactic polystyrene (PS, kindly supplied by Polimeri Europa). In particular, we used two PS matrices at different molecular weight, coded as PS-low (M_w=125 KDa; η_0=1.7*10^3 Pa*s at 200°C; τ_t≈0.1 s) and PS-high (M_w=268 KDa; η_0=2.1*10^4 Pa*s at 200°C; τ_t≈100 s), both having glass transition temperatures T_g=100°C.

Three kinds of nanoparticles were used as fillers: titanium dioxide (TiO_2 by Sigma Aldrich; density ρ=3.9 g/mL; surface area ~190÷290 m^2/g; average primary particles diameter d=15 nm) and alumina nanospheres (Al_2O_3 by Sigma Aldrich; ρ=4.00 g/mL; surface area: 35–43 m^2/g; d≈40 nm) were used to prepare PP/TiO_2 and PP/Al_2O_3 nanocomposites with filler volume fractions up to Φ=0.064; fumed silica (SiO_2 by Degussa; ρ=2.2 g/mL; surface area ~135-165 m^2/g; d=14 nm) was mixed with the two PS matrices up to Φ=0.041. PP/TiO_2 microcomposites were also prepared by using titanium dioxide microparticles (TiO_2 by Sigma Aldrich; ρ=3.9 g/mL; surface area ~0.14-0.04 m^2/g; d≈4 μm).

Nano- and microcomposites were prepared by melt compounding the constituents using a co-rotating extruder (Minilab Microcompounder, ThermoHaake) equipped with a capillary die (diameter 2 mm). The extrusions were carried out at 190°C. The screw speed was set to ~100 rpm, corresponding to an average shear rate of order of 50 s^{-1} inside the extrusion chamber. A feedback chamber allowed an accurate control of the residence time, which was

set to 250 s for all the samples. The polymer and the filler were previously dried under vacuum for sixteen hours at 70°C. The neat polymers used as reference materials were extruded in the same conditions to allow for an accurate comparison with the filled samples.

2.1.3 Characterization

The morphology of the composites was examined by transmission electron microscopy (TEM mod. EM 208, Philips). The observations were performed on slices with thickness ~150 nm, which were randomly cut from the extruded pellets using a diamond knife at room temperature.

Rheological tests were carried out by means of either a strain-controlled rotational rheometer (ARES L.S, Rheometric Scientific) or a stress-controlled rotational rheometer (ARG2, TA Instruments). The tests were carried out using parallel plates with diameter of 25 mm for the nanocomposites, while plates of 50 mm were used for the neat polymers because of their low viscosity. All measurements were performed in an atmosphere of dry nitrogen. The testing temperature was T=190°C for the PP/TiO_2 samples and T=200°C for the PS/SiO_2 samples. The viscoelastic moduli display a range of strain-independence, i.e. a range of linear viscoelasticity, which depends on the filler content. In order to determine the limits of the linear viscoelastic regime, oscillatory strain scans were performed on each sample at a fixed frequency of 0.063 rad s^{-1}. Low-frequency (ω=0.063 rad s^{-1}) time-sweep experiments were performed to study the evolution of the linear viscoelastic properties during time. The frequency-dependent elastic (G') and viscous (G'') moduli of the samples were measured by oscillatory shear scans in the linear regime. To account for the marked sensitivity of the rheological response on filler content, we evaluated the effective amount of filler of each sample used for the rheological experiments through thermogravimetrical analyses (TGA). The filler volume fraction Φ was estimated as:

$$\Phi = \frac{c\rho_p}{\rho_f + c(\rho_p - \rho_f)} \tag{3}$$

where c is filler weight fraction as deduced from TGA and ρ_p and ρ_f are the densities of polymer and filler, respectively.

2.1.4 Effect of the filler mobility on the linear viscoelasticity

The internal structure of the as extruded sample PP/TiO_2 at Φ=0.038 is shown in the TEM micrograph of Figure 1.a. Well distributed nanoparticle aggregates of a few hundreds of nanometers are suspended in the polymer matrix. The magnification of one of these aggregates is reported in Figure 1.b. A few hundreds of individual TiO_2 nanoparticles are closely packed into dense clusters with irregular shape.

The sample was subjected to a thermal annealing at 190°C in quasi-quiescent conditions, i.e. by submitting it to shear oscillations in the rheometer at small strain amplitude (γ=2%) and frequency (ω=0.063 rad s^{-1}). This allows to monitor the evolutions during time of slow dynamic populations, relaxing in timescales of order of $\tau=1/\omega\approx16$ sec, without altering the internal structure of the sample.

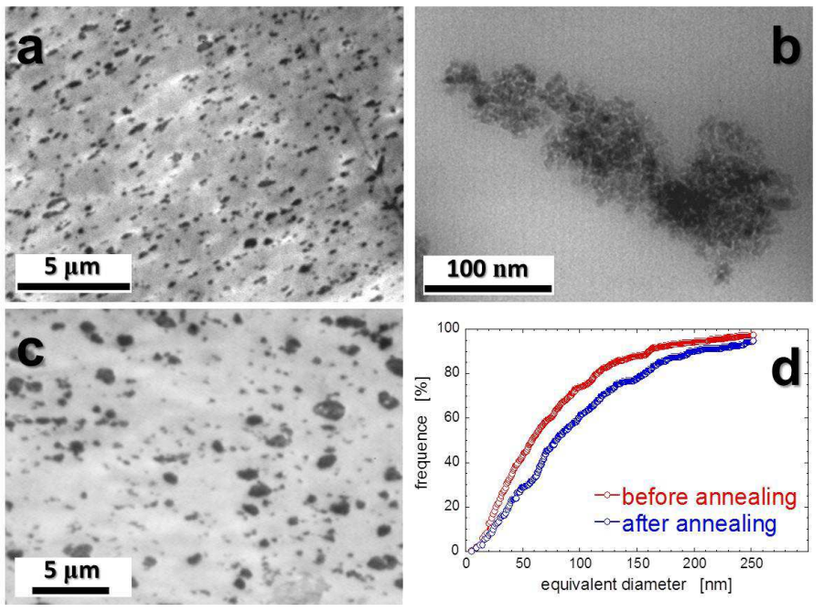

Fig. 1. (a) TEM micrograph of the as extruded sample PP/TiO_2 at Φ=0.045. (b) Magnification of an aggregate of TiO_2 nanoparticles. (c) TEM micrograph of the same sample as in (a) after a three-hours thermal annealing at T=190°C. (d) CSD of the samples shown in (a) and (c) (images taken from Acierno et al., 2007a).

The microstructure of the annealed sample is shown in Figure 1.c. A visual comparison with the morphology of the as extruded sample reveals the presence of bigger aggregates and the disappearance of the smaller ones. An analysis of the TEM micrographs was carried out to quantify the effect of the thermal annealing. An equivalent diameter for the aggregates was defined as $D_i=(\pi A_i)^{0.5}$, where A_i is the measured area of the i-th cluster. Once the sizes of the aggregates are available, the cumulative size distribution (CSD) and the number average size of the TiO_2 aggregates, $D_n=\Sigma n_i D_i/\Sigma n_i$ (n_i clusters with size D_i), was determined for each sample. The comparison between the CSDs is shown in Figure 1.d. The lowering of the cumulative CSD curves indicates an increase of the cluster sizes occurred during the thermal conditioning. In particular, the average size of the TiO_2 aggregates increases from D_n≈125 nm to D_n≈170 nm.

The coarsening of the microstructure is a consequence of the diffusion of the clusters under the push of Van der Waals attraction. Rheological parameters such as the linear viscoelastic moduli are extremely sensitive to the internal microstructure. Thus, we use them to follow such internal rearrangements. The time evolutions of G' and G'' at ω=0.063 rad s^{-1} are shown in Figure 2.

The elastic modulus, which at the beginning is lower than the viscous one, increases during the first stage and then it reaches a plateau after a certain time; on the other hand, the loss modulus remains essentially constant. Preliminary investigations revealed that the neat matrices display a constant value of the moduli in the analysed time window. Thus, the increase in the sample elasticity is related to the structuring of the inorganic phase. The characteristic timescale for such a phenomenon can be roughly estimated as the Smoluchowski

time for two clusters of radius R to come in contact, τ_a [Russel et al., 1989]. This characteristic time depends on on the self-diffusion time of each aggregate, given by Equation 2, and on the average inter-aggregates distance, inversely proportional to the filler amount:

$$\tau_a = \frac{\pi \eta_s R^3}{\overline{\Phi} k_B T} \tag{4}$$

$\overline{\Phi}$ is the actual filler volume fraction, i.e. the volume of the particles in a cluster plus the free volume enclosed between them. These regions are actually inaccessible to the polymer, and depends on how primary particles are assembled together inside the aggregates. As shown in Figure 1.b, the TiO_2 clusters appear rather compact. As a consequence, we can reasonably assume that the primary particles are packed at a volume fraction of ~60%, which is close to random close packing. The actual filler volume fraction of the PP/TiO_2 nanocomposites can be consequently estimated as $\overline{\Phi} \approx \Phi/0.6$. Assuming $R=D_n/2\approx65$ nm, Equation 4 gives $\tau_a \sim 4*10^3$ s, in good agreement with the data shown in Figure 2. This result suggests that the increasing of the sample elasticity during time is related to cluster-cluster aggregation. In order to support the previous conclusion, we increase τ_a by increasing either the size of primary particles or aggregates or the viscosity of the suspending medium. According to Equation 2, in these conditions we expect that the elasticity of the samples cannot increase significantly because of the reduced particle mobility.

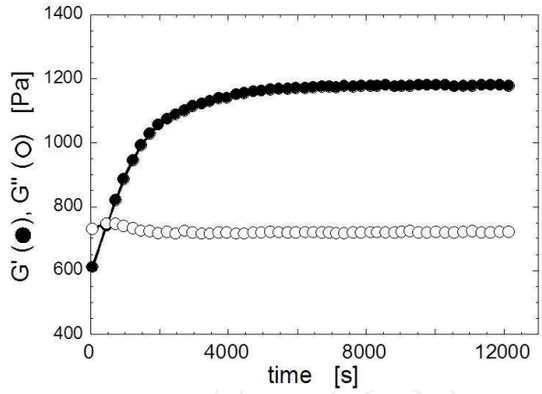

Fig. 2. Time evolution of G' (full) and G'' (empty) at ω=0.063 rad s^{-1} and T=190°C for the nanocomposite PP/TiO_2 at Φ=0.038 (image taken from Romeo et al., 2009).

As first test, we investigate the time evolutions of the linear viscoelastic moduli at ω=0.063 rad s^{-1} for a PP/TiO_2 microcomposite (particles radius $R\approx2$ μm) at $\Phi\approx0.035$. Based on Equation 4, we expect that two micron-sized particles should come at contact after timescales of order of ~10^7 s. As a matter of fact, the results shown in Figure 3.a indicate that both moduli remain stable during the aging test until ~10^4 s.

As second test, we monitor the moduli of a nanocomposite based on a high viscosity matrix such as PS-high (η_0=2.1*10^4 Pa*s at 200°C) filled with SiO_2 particles at $\Phi\approx0.035$. Silica aggregates exhibits the typical open and branched structure of fractal objects. In such systems the mass M scales with length L as $M\sim L^{d_f}$, d_f being the fractal dimension [Weitz & Oliveira, 1984]. The actual filler volume fraction thus becomes [Wolthers et al., 1997]:

$$\overline{\Phi} = \Phi \times (L / d)^{3-d_f} \tag{5}$$

Setting $L=D_n\approx125$ nm as emerged from the analysis of many TEM micrographs, and taking d_f=2.2 as a typical fractal dimension of fumed silica aggregates [Kammler et al., 2004], Equation 4 gives $\tau_a\sim10^5$ s. This is in agreement with the results of the time sweep experiment shown in Figure 3.b, which indicate that cluster assembling phenomena, if any, are negligible in the timescale of the test. Obviously, the not structured sample keeps a predominantly viscous connotation, i.e. $G''>>G'$.

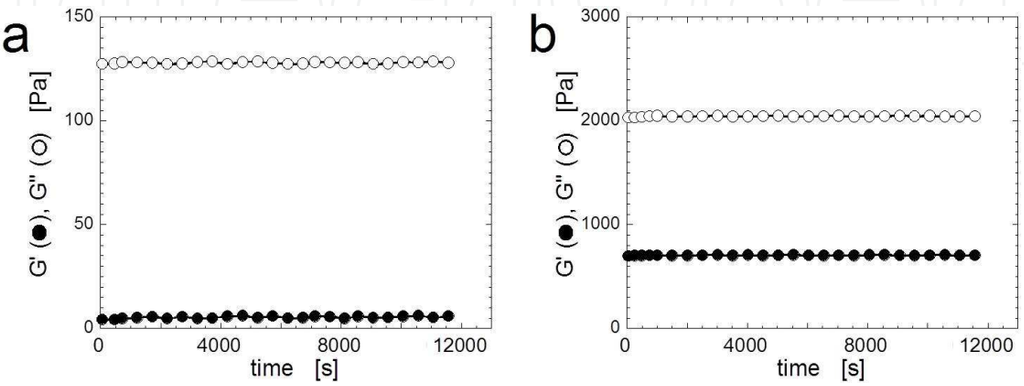

Fig. 3. Time evolution of G' (full) and G'' (empty) at ω=0.063 rad s^{-1} for the microcomposite PP/TiO_2 at Φ=0.035 and T=190°C (a), and the nanocomposite PS-high/SiO_2 at Φ=0.035 and T=200°C (b) (images taken from Romeo et al., 2009).

Particle rearrangements eventually give rise to mesoscopic structures, such as branched aggregates or space-spanning filler network, which strongly alter the frequency response of the sample. The ω-dependent G' and G'' of two PP/TiO_2 samples filled with micro- and nanoparticles both at $\Phi\approx0.035$ are compared in Figure 4.a. In both cases the matrix governs the high-frequency response. This suggests that the relaxation modes of the polymer chains and sub-chains are only slightly affected by the presence of the filler at these high frequencies. The presence of microparticles negligibly affects the whole response of the composite. On the contrary, the nanoparticles significantly alter the low-frequency moduli of the material, and in particular the elastic one.

The flattening of G' over long timescales is a general feature characterizing different kinds of PNCs [Krishnamoorti & Yurekli, 2001; Du et al., 2004]. Such a behaviour, however, is not a direct consequence of the nanometric size of the particles, but rather it originates from particle mobility. To emphasize this point, in Figure 4.b the frequency response of the three-hours aged samples PS-low/SiO_2 and PS-high/SiO_2 at $\Phi\approx0.035$ are compared. The nanocomposite with high viscosity matrix displays a liquid-like behaviour at low frequency reminiscent of that of the neat polymer (not shown). Differently, the PS-low/SiO_2 sample exhibits a predominant elastic connotation, the low-frequency plateau of G' being indicative of the presence of a space-spanning filler network formed during the ageing process.

To summarize, the viscoelastic response of a filled polymer is greatly affected by particle mobility. When the characteristic diffusion time of the particles and/or aggregates resulting from the extrusion process is too high, either because the matrix is too viscous or the particle

size is too big, the filler is unable to rearrange and only produce a small perturbation of the composite viscoelastic response. Conversely, when mobility of the inorganic phase is high enough, random motion and attractive Van der Waals forces lead to the structuring of the primary aggregates. This eventually results in the formation of a whole space-spanning filler network. Since this network exhibits the connotation of an elastic solid, a drastic slowing down of relaxation dynamics occurs at low frequencies.

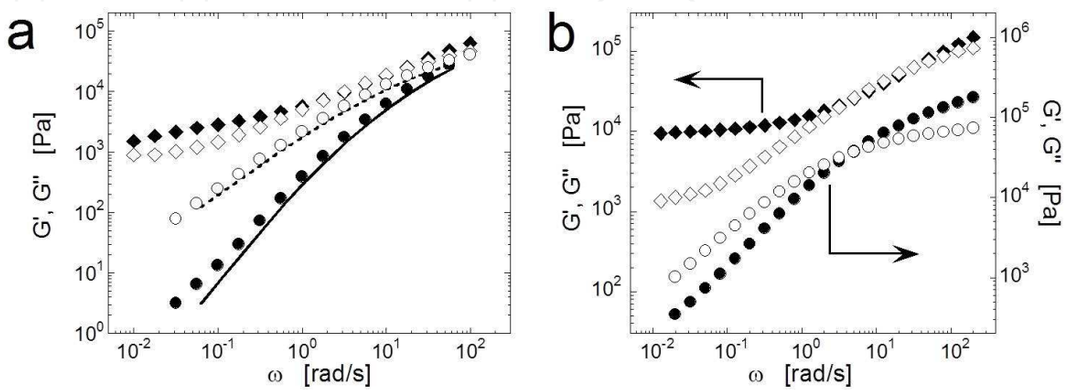

Fig. 4. (a) G' (full) and G'' (empty) for the samples PP/TiO_2 at $\Phi \approx 0.035$ filled with micrometric (circles) and nanometric (diamonds) particles. Solid and dashed lines represent the elastic and viscous modulus of the neat PP, respectively. (b) G' (full) and G'' (empty) for the nanocomposite samples PS-low/SiO_2 (diamonds, left axis) and PS-high/SiO_2 (circles, right axis) at $\Phi \approx 0.035$ (image taken from Romeo et al., 2009).

2.2 Linear viscoelasticity of PNCs

2.2.1 Weakly attractive particles suspended in Newtonian fluids – A two-phase model

Colloids are typically nanometer to micron sized particles forming a dispersed phase in a suspending medium. Colloidal dispersions exhibit a wide spectrum of rheological properties, ranging from simply viscous fluids to highly elastic pastes depending on the amount of particles and the sign and magnitude of inter-particles interactions. Here we are interested in weakly attractive systems, where the particles are inclined to assemble together into more or less branched flocs. In these systems, the ω-dependent storage and loss modulus typically exhibit a strong dependence on both Φ and U. Such a high variability makes extremely difficult a general description of the viscoelastic behaviour of colloidal dispersions. A drastic simplification has been introduced by Trappe and Weitz, which showed that modelling the suspension above the particle percolation threshold as an elastic filler network interspersed in a background fluid (two-phase model) qualitatively accounts for the viscoelasticity of their samples [Trappe & Weitz, 2000]. The authors studied a dispersion of carbon black in base stock oil as a function of particle volume fraction and interaction potential. The U was tuned by adding a dispersant that acts as a surfactant. Without dispersant carbon black particles are rather strongly attractive, and flocs of ~100 μm in size form even at very low amounts of particles. The linear viscoelastic moduli of samples at different Φ were measured as a function of frequency with a strain-controlled rheometer with Couette geometry. The authors found that a rheological transition occurs at Φ_c=0.053: at $\Phi > \Phi_c$ the suspension is clearly elastic and G' is nearly independent on ω; at

$\Phi<\Phi_c$ the viscous feature definitely prevails over the elastic one, and the suspension rheology looks like that of the suspending fluid. Microscopic analyses reveal that the rheological transition reflects the state of dispersion of the filler: isolated carbon black flocs are suspended in the background fluid below Φ_c, whereas above this threshold the aggregates assemble in a three-dimensional space spanning network.

Despite their marked differences, the moduli of the samples at $\Phi>\Phi_c$ can be scaled onto a single pair of master curves. The authors qualitatively accounted for the observed scaling by assuming that the carbon black forms a solid but tenuous network with a purely elastic, ω-independent modulus. The elasticity of this network, G'_0, increases with Φ as the network becomes more and more robust. Interspersed throughout this structure is the purely viscous suspending fluid, which G'' linearly increases with ω and is substantially independent of Φ. Consequently, the elasticity of the network prevails at low ω, while the viscosity of the fluid dominates at high ω. Within this simplified picture, scaling the elasticity of each sample along the viscosity of the matrix results in the collapse of data of samples at different composition onto a single pair of master curves.

Although the proposed approach can account for the basic scaling behaviour, many issue remain unresolved. For example, the behaviour of the weaker of the two moduli in each regime is not addressed. At low frequencies, $G''(\omega)$ must be determined by the loss modulus of the network, which is larger than that of the suspending fluid. Similarly, at the highest frequencies $G'(\omega)$ must reflect the storage component of the suspending fluid with the solid network in it. In addition, the model does not take into account hydrodynamic effects. Despite these limitations, the good quality of the scaling supports the reliability of the approach, indicating that there is a strong similarity in the structures of the networks that form at different Φ. This also implies some predictive feature of the model: the tiny elasticity of samples at low Φ (as long as greater than Φ_c), which networks are too tenuous to be appreciated through direct dynamic-mechanical analyses, can be predicted with good approximation by simply referring to the master curve of G'.

2.2.2 Weakly attractive nanoparticles suspended in non-Newtonian mediums – Recovering the two-phase model

The relatively high mobility of nanoparticles even in highly viscous fluids such as polymer melts makes PNCs similar to colloidal dispersions. The main difference with these simpler systems is the non-Newtonian feature of the suspending medium. According to Trappe and Weitz, the viscoelasticity of a colloidal suspension above Φ_c originates from the combination of the responses of an *elastic* particle gel that of the *purely viscous* background fluid. In the case of a PNC, instead, the suspending medium is viscoelastic by itself, and its response combines with that of the space-spanning network giving rise to a more complex ω- and Φ-dependent viscoelastic behaviour. It follows that a separation of the effects of the solid and fluid phases is no more possible in the case of PNCs. However, we argue that a recovery of the two-phase model is possible if the elasticity of the polymer is neglected with respect to that of the filler network. Under this assumption, the viscoelasticity of the PNC can be split into the independent responses of an *elastic* particle network and that of the *predominantly viscous* polymer. The former contribution depends on the filler content and governs the long timescale response of the composite, whereas the latter is responsible for the high-frequency behaviour (Figure 5).

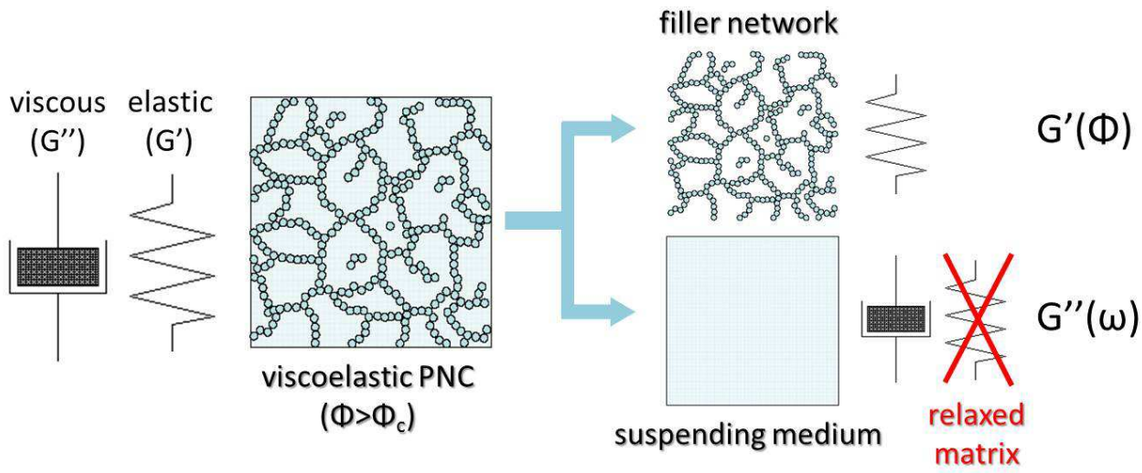

Fig. 5. Scheme of the viscoelasticity of a PNC at $\Phi > \Phi_c$. For fully relaxed polymer matrix, the filler network is the only responsible for the elastic connotation of the system.

To test the validity of the previous considerations, we focus on the ω-dependence of the moduli of PP/TiO_2 and PS-low/SiO_2 nanocomposite samples at $\Phi > \Phi_c$, i.e. in which the filler rearranges in experimentally accessible timescales forming a space-spanning network. All these samples share a similar pseudo solid-like behaviour at low frequency, with weak ω-dependences of both moduli and G' greater than G''. Since the filler mainly affects the elastic modulus of the samples, G' increases with Φ more rapidly than G''. As a consequence, a further crossover between G' and G'' occurs at intermediate frequencies in addition to that at high ω related to the relaxation of the neat polymer. The coordinates of such additional crossing point, (ω_c; G_c), shift towards higher and higher frequencies and moduli with increasing the filler content. This is shown in Figure 6 for three samples PS-low/SiO_2 at different composition.

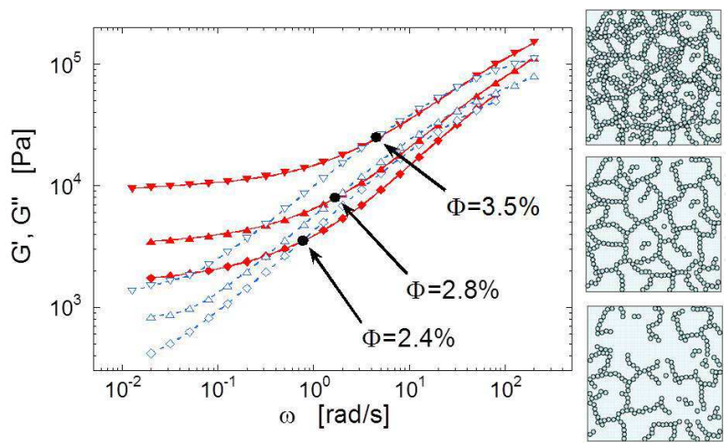

Fig. 6. G' (full, red) and G'' (empty, blu) for the nanocomposite samples PS-low/SiO_2 at increasing filler content. The additional crossover is indicated by the arrows.

The additional low-frequency crossover can be interpreted as the point at which the network elasticity equals the viscous contribution of the polymer. As a consequence,

normalizing the moduli of samples at different Φ by their elasticity, and doing so along the background fluid viscosity, the curves should collapse onto a single pair of master curves. Accordingly, the scaling has to be done by shifting the curves both horizontally and vertically using as shift factors $a=1/\omega_c$ and $b=1/G_c$, respectively. The resulting master curves are shown in Figure 7 for both the PP/TiO_2 and PS-low/SiO_2 nanocomposites.

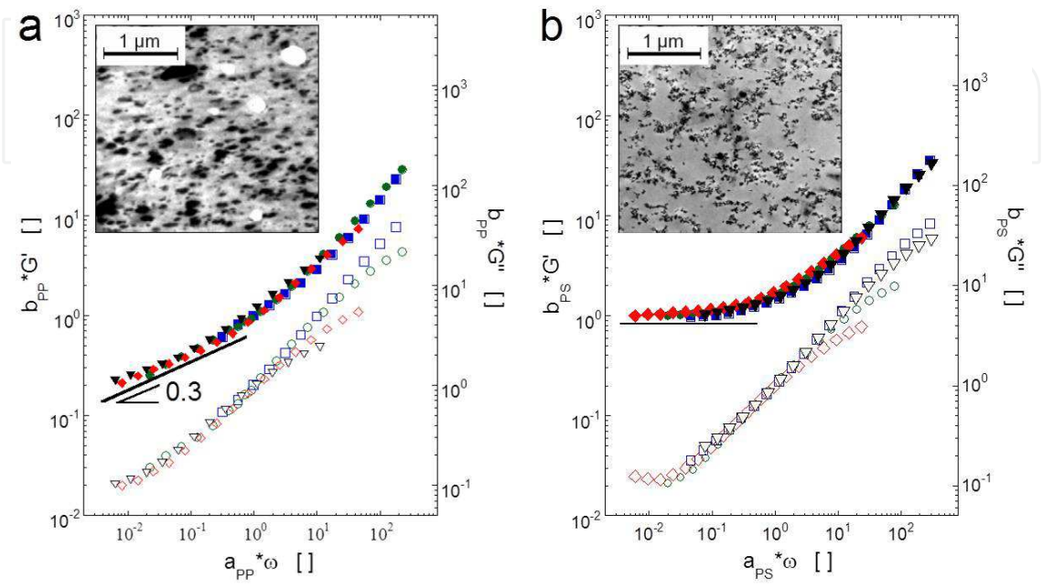

Fig. 7. Master curves of G′ (full, left axis) and G″ (empty, right axis) for the systems PP/TiO_2 (a) and PS-LOW/SiO_2 (b). Each colour corresponds to a composition. Note that only curves at $\Phi>\Phi_c$ have been used to build the master curves. The TEM micrographs shown in the insets represent the microstructures of samples at $\Phi\approx0.035$ (image taken from Romeo et al., 2009).

The scaled moduli lie on top of each other in about five decades of frequencies, supporting the validity of the adopted approach. Deviations are observed for the viscous moduli at high scaled frequencies. This is not unexpected, since the relaxation modes of the polymers are independent on the filler content and cannot be scaled using a and b as scaling factors.

Once the master curves are built, the differences in elasticity and dynamic of the particle networks become evident. The SiO_2 network is characterized by an ω-independent elastic modulus at low frequency, which emphasizes its truly solid-like feature. Differently, the TiO_2 network displays a slow relaxation dynamic with $G'\sim\omega^{0.3}$. These differences are related to the differences in network structures formed in the two composites. The TEM images reported in the insets of Figure 7 show that the SiO_2 nanoparticles form a tenuous, fractal network of sub-micron sized, branched flocs interspersed within the host PS. Differently, the TiO_2 nanoparticles are assembled into dense clusters, which mobility is presumably slowed down by the surrounding aggregates. The transient character of the latter network emerges as a glassy-like decrease of G', which reflects the internal rearrangements of the TiO_2 clusters. Such slow relaxation dynamics are characteristic of colloidal glasses [Shikata & Pearson, 1994; Mason & Weitz, 1995] and has been observed in many other soft materials [Sollich et al., 1997].

2.2.3 Refining the two-phase model – Role of the hydrodynamic effects

Despite the good quality of the scaling shown in Figure 7, unresolved issues exist regarding the physical meaning of the shift factors. The underlying physics of the model lies on the independent rheological responses of the *neat polymer* and the particle network. Actually, the coordinates of the crossover point of the moduli of the nanocomposite, identified by Trappe and Weitz as the shift factors for their system, do not rigorously reflect the properties of the two pristine phases of the model. In addition, the presence of the particles implies hydrodynamic effects, which cannot be eluded for a correct scaling of the data. To account for these issues, the procedure to get the shift factors for the building of the master curve has to be revisited. For this aim, hereinafter we only refer to the system PS-low/SiO_2, which particle network exhibits a truly solid-like behaviour at low frequency.

Hydrodynamic effects reflect the perturbation of the flow lines in proximity of the filler. In a liquid filled with a solid particulate, the suspending fluid flows in the narrow gap between contiguous particles or aggregates, locally experiencing a greater flow rate than what externally imposed or measured. Gleissle and Hochstein quantitatively accounted for hydrodynamic effects in oscillatory shear experiments by introducing an empiric amplification factor, representing the ratio between the complex moduli of the filled sample over that of the neat matrix: $B(\Phi) = G^*(\Phi)/G^*_{PS}$ [Gleissle & Hochstein, 2003]. In the case of microparticles, $B(\Phi)$ well describe the increase of G^* of the suspension in the whole range of accessible frequencies. Differently, non-continuum effects emerge over long timescales in the case of PNCs. Consequently, the hydrodynamic effects only are appreciable at high frequencies, i.e. where the rheological response is governed by the polymer matrix. This is shown in Figure 8, where the complex moduli of various PS-low/SiO_2 nanocomposites at different composition are reported together with the resulting $B(\Phi)$.

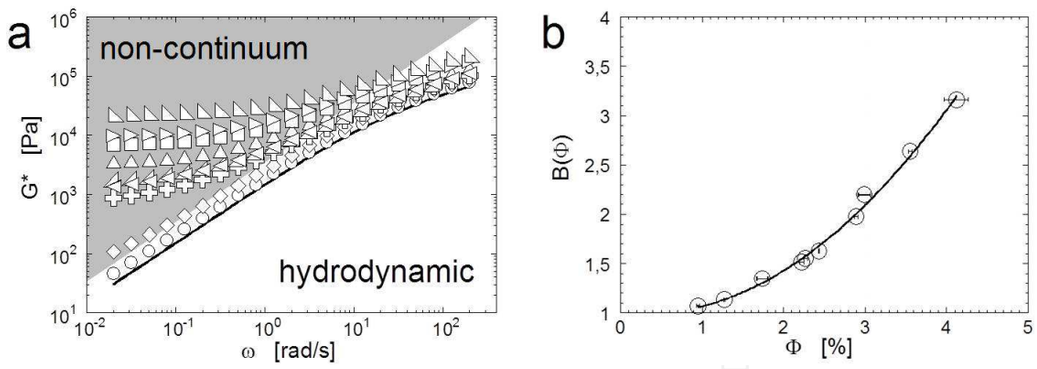

Fig. 8. (a) Complex modulus of PS-low/SiO_2 nanocomposite at various filler content. The regions in which non-continuum and hydrodynamic effects are dominant are emphasized. (b) Amplification factor for the data shown in (a) (images taken from Filippone et al., 2010).

After the hydrodynamic contribution has been quantified for each sample, then new and more rigorous shift factors can be identified. Specifically, we now refer to the point at which the elasticity of the filler network, given by the plateau modulus of the nanocomposite, $G'_0(\Phi)$, equals the viscous modulus of the neat matrix amplified by $B(\Phi)$ to account for hydrodynamic effects, $B(\Phi)\cdot G^*$.

The comparison between the old (a; b) and new (a'; b') shift factors is shown in Figure 9.a for the sample at Φ=2.9%; in Figure 9.b the new master curve is reported.

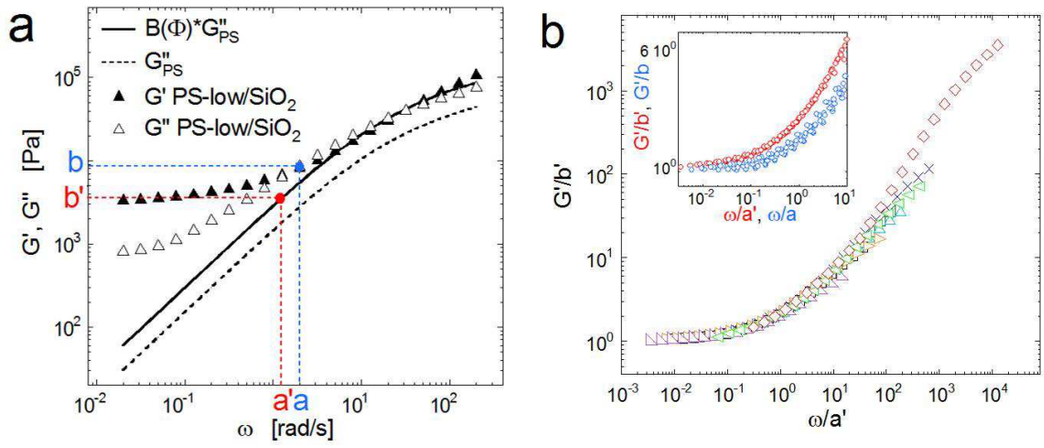

Fig. 9. (a) Comparison of the shift factors for the samples-low/SiO_2 at Φ=2.8%. (b) Master curve of G′ built using a′ and b′ as shift factors; the inset shows a magnifications at low scaled frequencies of the master curves obtained using as shift factors (a′; b′) (red) and (a; b) (blu) (images taken from Filippone et al., 2010).

The elastic moduli scaled using a' and b' as shift factors lies on top of each other over about seven decades of scaled frequencies, confirming the validity of the adopted approach. Again, the slight deviations at ω/a' greater than ~10^1 do not invalidate the consistency of the scaling, being a consequence of the intrinsic viscoelastic feature of the suspending fluid.

Besides exactly capturing the underlying physics of the two-phase model, the refined model guarantees a better scaling of the elasticity of samples at different composition. This is shown in the inset of Figure 9.b, where the master curves built using the two pairs of shift factors are compared. The lower scattering of the data scaled using a' and b' confirms the importance of properly accounting for hydrodynamic contributions when dealing with PNCs.

2.3 Strength and reversibility of the filler network in PP/Al_2O_3 PNCs

Aim of this paragraph is the study of the relationships between the rheology and structure of PP/Al_2O_3 nanocomposites. The structuring (during a quiescent annealing process) and de-structuring (promoted by large amplitude shear flows) of the filler network are investigated by means of both rheological and TEM analyses. The internal morphology of the sample PP/Al_2O_3 at Φ=4.2% at the end of the extrusion process is shown in Figure 10.

Although a homogeneous distribution can be observed on microscale, the presence of aggregates of a few hundred nanometers is noticed at higher magnifications. The aggregates appear as open structures formed of tens of nanospheres of different sizes. Such non-equilibrium structures rearrange towards a more favourable thermodynamic state during a subsequent aging above the PP melting temperature. The morphology of a sample at Φ=4.2% after a 3-hours annealing at T=190°C is shown in Figure 11.

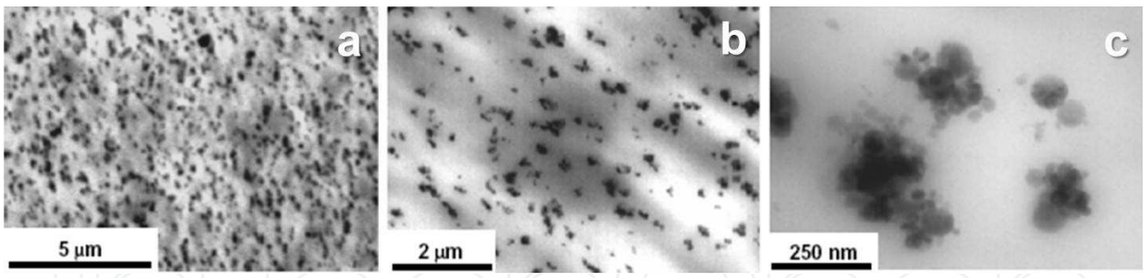

Fig. 10. TEM micrographs of the as extruded PP/Al_2O_3 sample at Φ=4.2% at various magnifications (image taken from Acierno et al., 2007b).

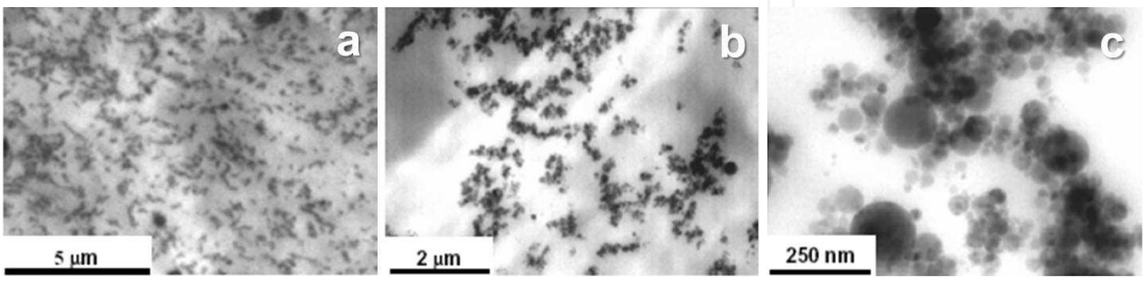

Fig. 11. TEM micrographs of the 3-hours thermal annealed PP/Al_2O_3 sample at Φ=4.2% at various magnifications (image taken from Acierno et al., 2007b).

Pristine individual aggregates are now assembled into a disordered network that spans large sections of the sample. The particles and aggregates are essentially kept together by Van der Waals attractions and/or other kinds of weak bonds between the functional sites located at the particle surfaces. The application of large strains provides an excess energy to overcome such attractive interactions, thus destroying the network. After that, the particles may or may not aggregate again depending on the strength of inter-particle interactions.

The relaxation dynamics of a viscoelastic fluid can be indifferently monitored by frequency scans or stress relaxation tests. In the latter kind of experiment, a constant strain, γ_0, is imposed to the sample in the linear regime, and the transient stress, $\sigma(t)$, is measured as a function of time. The stress relaxation modulus, $G(t)=\sigma(t)/\gamma_0$, is shown in Figure 12 after the application of large amplitude oscillatory shear (LAOS) at a constant frequency ω=0.0628 rad s^{-1} and different γ_0 on the 3-hours aged sample at Φ=4.2%.

Large deformations have a drastic effect on the relaxation spectrum: the bigger the strain amplitude, the faster the relaxation dynamics. Time sweep tests in linear regime were performed after each LAOS to test the viscoelastic behaviour of the sheared sample, and the results are shown in the inset of Figure 12. The elastic feature progressively vanishes with increasing the deformation amplitude. Interestingly, the steadiness of the elastic modulus during time suggests an irreversibility of the network break-up process, at least within the experimental time window. Moreover, a polymer-like behaviour is recovered after the LAOS at the largest amplitude (γ_0=500%). In such case, the inorganic phase does not affect the rheological response of the nanocomposite at all.

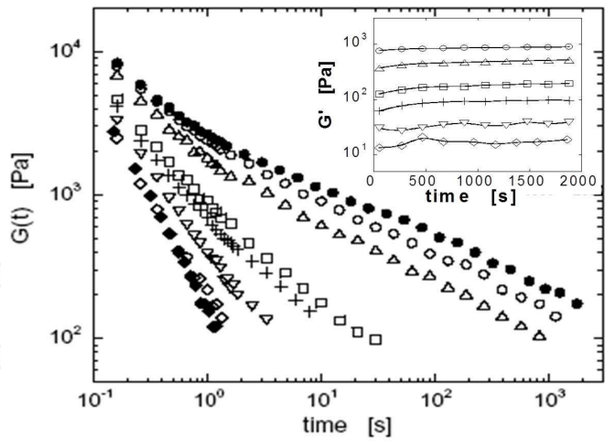

Fig. 12. $G(t)$ of the 3-hours aged PP/Al_2O_3 sample at Φ=4,5% after LAOS at different strain amplitudes γ_0: 0.8% (solid circles), 10% (open circles), 25% (triangles), 50% (squares), 100% (crosses), 250% (reverse triangles), 500% (diamonds). Solid diamonds represents the $G(t)$ of the neat polymer. The time evolutions of G' after each LAOS are shown in the inset. Symbols are the same of stress relaxation moduli (image taken from Acierno et al., 2007b).

The morphology of the 3-hours aged sample after the LAOS at γ_0=500% is reported in Figure 13. The network formed during aging is no more visible, and the presence of many small clusters characterizes the sheared system. The flocs show a more open structure than that of a not sheared sample, either aged or not, suggesting a weaker tendency to the clustering for the Al_2O_3 nanoparticles after the large deformations. The cumulative cluster size distributions were determined through the analysis of TEM micrographs. The results are shown in Figure 14 for the as extruded, 3-hours annealed and sheared after aging samples at Φ=4.2%. The number average equivalent diameters of the clusters are reported in the same figure.

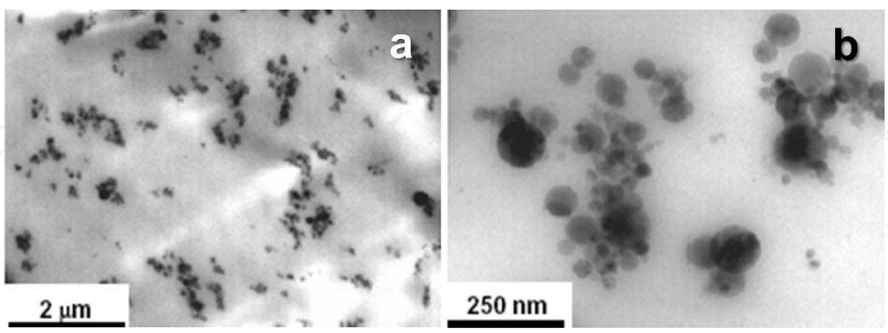

Fig. 13. TEM morphology of the 3-hours aged sample at Φ=4.2% after the LAOS at γ=500% (image taken from Acierno et al., 2007b).

The CSD of the as extruded sample is rather sharp, indicating a good dispersion efficiency of the extrusion process. The thermal annealing results in a significant widening of the CSD, with the appearance of very large clusters (D_n greater than 800 nm). This confirms the metastable feature of the samples, which quickly evolve toward states of less free energy

under the push of the inter-particle attractive interactions. The resulting filler network breaks up when the sample is subjected to LAOS, and a remarkable sharpening of the CSD is observed.

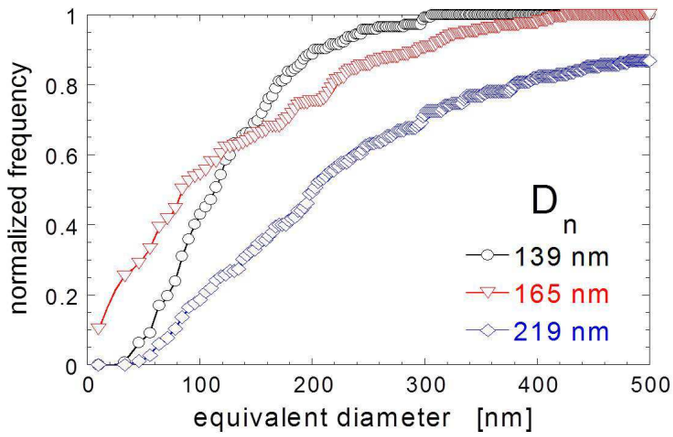

Fig. 14. CSDs for the PP/Al_2O_3 sample at Φ=4.2% as extruded (black circles), 3-hours aged (blue diamonds) and 3-hours aged after LAOS at γ_0=500% (red triangles) (image taken from Acierno et al., 2007b).

Interestingly, the strength of the filler network depends on whether the LAOS is applied before or after the thermal annealing. This is shown in Figure 15, where the loss factor $tan\delta=G''/G'$ (15.a) and the complex moduli (15.b) of the samples at Φ=4.2% submitted to LAOS (γ_0=500%) are reported before and after the ageing; the curves of the 3-hours aged but not sheared sample are also reported for comparison.

If the LAOS is applied to the sample before the formation of the particle network, the system quickly evolves to a more elastic structure and the $tan\delta$ asymptotically reaches values close to those of the not sheared sample. However, the comparison between the G^* shown in

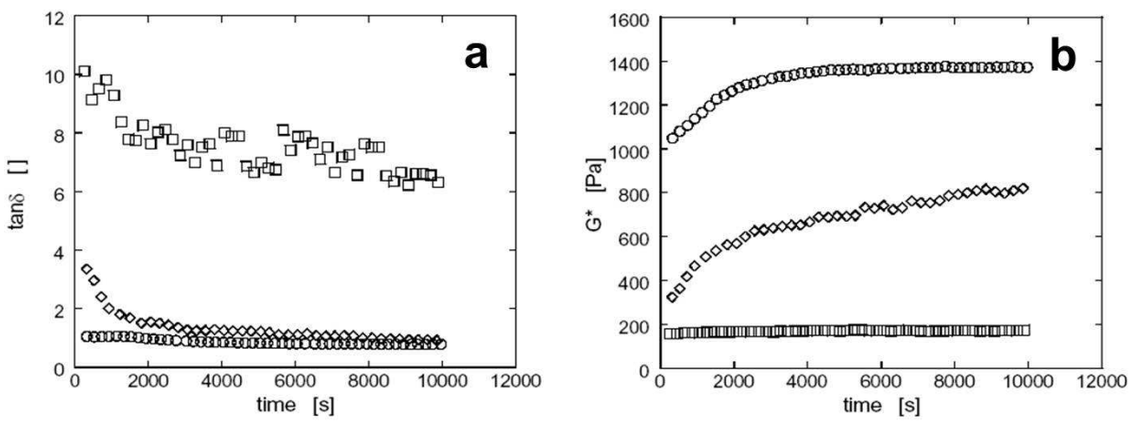

Fig. 15. Loss factor (a) and complex moduli (b) of the samples at Φ=4.2% submitted to LAOS (γ_0=500%) before (diamonds) and after (squares) the thermal annealing. The curves of the 3-hours aged and not sheared sample (circles) are also reported for comparison (image taken from Acierno et al., 2007b).

Figure 15.b reveals that the strength of the network formed after the LAOS is much lower than that of the not sheared sample.

Such a result can be explained by assuming some rearrangement of the reactive sites of the particle surfaces after the network break-up, which may weaken the surface activity of the particles. This reduces the intensity of inter-particle interactions and, as a consequence, the strength of the filler network [Bicerano et al., 1999]. On the other hand, if a "strong" network forms and then it is destroyed by LAOS, the restoration of new bonds required for the reformation of the network can results inhibited. This could explain the irreversibility of the structuring process noticed after the LAOS performed on the aged sample.

3. Conclusions

The effect of small amounts of nanoparticles on the melt-state linear viscoelastic behaviour has been investigated for different polymer-nanoparticles model systems characterized by poor polymer-particles interactions and low particle contents. The drastic increase of the rheological properties with respect to the matrices has been related to the formation of a filler network above a critical particles volume fraction. This is a consequence of particles and clusters rearrangements taking place during a thermal annealing. The filler mobility depends on both particle size and viscosity of the suspending medium. Once formed, the filler network exhibits an elastic feature that mixes with the intrinsic viscoelastic response of the polymer matrix, resulting in a complex Φ- and ω-dependent viscoelastic response of the nanocomposite. However, starting from a two-phase model proposed for colloidal suspensions in Newtonian fluids, we have shown that the contributions of filler network and suspending medium can be decoupled due to the weak polymer-particle interactions and the differences in temporal relaxation scales. The adopted approach has been validated through the building of a master curve of the moduli, which reflects the scaling of the elasticity of composites along the viscosity of the suspending medium. The two-phase model well works irrespective of the structure of the filler network, making evident the strict interrelationships between the structure, both on nano- and micro-scale, and the melt-state behaviour of the studied PNCs. The physical meaning of the two-phase model clearly emerges once hydrodynamic effects have been properly taken into account. Besides clarifying the various timescales of PNCs, the proposed model allows for predicting the modulus of particle networks which are too tenuous to be appreciated through simple frequency scans. The application of a large amplitude oscillatory shear flows provides an excess energy for the system to escape from the metastable configuration in which it is trapped. This destroys the network formed during the thermal annealing, leading to a more tenuous structure which is unable to significantly contribute to the system elasticity. After the network has been destroyed the sample cannot recover its previous solid-like feature during a subsequent thermal annealing. This is probably due to some rearrangement of the reactive sites of the particle surfaces occurring after the rupture of the inter-particles bonds formed during annealing.

Besides well describing the behaviour of PNCs in the framework of simpler systems such as Newtonian colloidal suspensions, the analysis proposed in this chapter is expected to be useful to understand a wide variety of complex fluids in which a superposition of the elasticity of the components is possible. The generalization of our approach to such systems

and to other technologically relevant PNCs, such as nanocomposites based on layered silicates or carbon nanotubes, still remains to be proved.

4. References

Acierno, D.; Filippone, G.; Romeo, G.; Russo, P. (2007). Rheological aspects of PP-TiO_2 nanocomposites: a preliminary investigation. *Macromol. Symp.*, Vol. 247, pp. 59-66

Acierno, D.; Filippone, G.; Romeo, G.; Russo, P. (2007). Dynamics of stress bearing particle networks in poly(propilene)/alumina nanohybrids, *Macromol. Mater. Eng.*, Vol. 292, pp. 347-353

Baird, D. G.; Collias D. I. (1995). In: *Polymer Processing Principles and Design*, John Wiley and Sons, Inc., ISBN: 978-0-471-25453-9, New York (USA)

Bicerano, J.; Douglas, J. F.; Brune, D. A. (1999). Model for the viscosity of particle dispersions. *J. Macromol. Sci.: Rev. Macromol. Chem. Phys.* Vol. 39, No. 4, pp. 5611-642

Cipelletti, L.; Manley, S.; Ball, R. C.; Weitz, D. A. (2000). Universal aging features in restructuring of fractal colloidal gels. *Phys. Rev. Lett.*, Vol. 84, No. 10, pp. 2275-2278

Du, F.; Scogna, R. C.; Zhou, W.; Brand, S.; Fischer, J. E.; Winey, K. I. (2004). Nanotube networks in polymer nanocomposites: rheology and electrical conductivity, *Macromolecules*, Vol. 37, pp. 9048-9055

Filippone, G.; Romeo, G.; Acierno, D. (2010). Viscoelasticity and structure of polystyrene/fumed silica nanocomposites: Filler Network and Hydrodynamic Contributions. *Langmuir*, Vol. 26, No. 4, pp. 2714–2720

Gleissle, W.; Hochstein, B. (2003). Validity of the Cox–Merz rule for concentrated suspensions. *J. Rheol.*, Vol. 47, pp. 897-910

Inoubli, R.; Dagréou, S.; Lapp, A.; Billon, L.; Peyrelasse, J. (2006). Nanostructure and mechanical properties of polybutylacrylate filled with grafted silica particles. *Langmuir*, Vol. 22, No. 15, pp. 6683-6689

Israelachvili, J. (1991). In: *Intermolecular and surface forces*, Academic Press, ISBN 0-12-375181-0, London, UK

Jancar, J.; Recman, L. (2010). Particle size dependence of the elastic modulus of particulate filled PMMA near its T_g, *Polymer*, Vol. 51, No. 17, (August 2010), pp. 3826-3828

Kammler, H. K.; Beucage, G.; Mueller, R.; Pratsinis S. E. (2004). Structure of flame-made silica nanoparticles by ultra-small-angle X-ray scattering. *Langmuir*, Vol. 20, pp. 1915-1921

Kojima Y, Usuki A, Kawasumi M, Okada A, Fukushima Y, Kurauchi T, Kamigaito O. (1993) Mechanical properties of nylon 6-clay hybrid, *J Mat Res* Vol. 8, pp. 1185-1189

Krishnamoorti, R.; Yurekli, K. (2001). Rheology of polymer layered silicate nanocomposites, *Curr. Opin. Colloid Interface Sci.* Vol. 6, No. 5-6, pp. 464-470

Mason, T. G.; Weitz, D. A. (1995) Linear viscoelasticity of colloidal hard sphere suspensions near the glass transition. *Phys. Rev. Lett.*, Vol. 75, pp. 2770-2773

Ozmusul, M. S.; Picu, R. C.; Sternstein, S. S.; Kumar, S. (2005). Lattice Monte Carlo simulations of chain conformations in polymer nanocomposites , *Macromolecules*, Vol. 38, No. 10, pp. 4495-4500

Prasad, V.; Trappe, V.; Dinsmore, A. D.; Segrè, P. N.; Cipelletti, L.; Weitz, D. A. (2003) Universal features of the fluid to solid transition for attractive colloidal particles. *Faraday Discuss.*, Vol. 123, pp. 1-12

Pusey, P. N.; van Megen, W. (1986). Phase behaviour of concentrated suspensions of nearly hard colloidal spheres. *Nature*, Vol. 320, pp. 340-342

Ren, J.; Silva, A. S.; Krishnamoorti, R. (2000). Linear viscoelasticity of disordered polystyrene−polyisoprene block copolymer based layered-silicate nanocomposites. *Macromolecules*, Vol. 33, No. 10, pp. 3739-3746

Romeo, G.; Filippone, G.; Fernández-Nieves, A.; Russo, P.; Acierno, D. (2008). Elasticiy and dynamics of particle gels in non-Newtonian melts. *Rheol. Acta*, Vol. 47, pp. 989-997

Romeo, G.; Filippone, G.; Russo, P.; Acierno, D. (2010). Effects of particle dimension and matrix viscosity on the colloidal aggregation in weakly interacting polymer-nanoparticle composites: a linear viscoelastic analysis. *Polym. Bull.*, Vol. 63, No.6, pp. 883-895

Russel, W. B.; Saville, D. A.; Schowalter, W. R. (1989). In: *Colloidal dispersions*, Cambridge University Press, ISBN 0-521-34188-4, Cambridge, UK

Saint-Michel, F.; Pignon, F.; Magnin, A. (2003). Fractal behavior and scaling law of hydrophobic silica in polyol. *J. Colloid* space *face Sci.*, Vol. 267, No. 2, pp. 314-319

Shenoy, A. V. (1999). In: *Rheology of filled polymer systems*, Kluwer Academic Publishers, ISBN 0-4112-83100-7, Dordrecht, The Netherlands

Shikata, T.; Pearson, D.S. (1994). Viscoelastic behavior of concentrated spherical suspensions. *J. Rheol.*, Vol. 38, pp. 601-613

Sollich, P.; Lequeux, F.; Hébraud, P.; Cates, M. E. (1997). Rheology of soft glassy materials. *Phys. Rev. Lett.* 78, 2020-2023

Surve, M.; Pryamitsyn, V.; Ganesan, V. (2006). Universality in structure and elasticity of polymer-nanoparticle gels. *Phys. Rev. Lett.*, Vol. 96, No. 17, pp. 1778051-1778054

Trappe, V.; Weitz, D. A. (2000). Scaling of the viscoelasticity of weakly attractive particles. *Phys. Rev. Lett.*, Vol. 85, No. 2, pp. 449-452

Trappe, V.; Prasad, V.; Cipelletti, L.; Segrè, P.N.; Weitz, D. A. (2001). Jamming phase diagram for attractive particles. *Nature*, Vol. 411, pp. 772-775

Usuki A.; Kojima Y.; Kawasumi M.; Okada A.; Fukushima Y.; Kurauchi T.; Kamigaito O. (1993). Synthesis of nylon 6-clay hybrid. *J Mat Res*, Vol. 8, pp. 1179-1184

Weitz, D. A.; Oliveira, M. (1984). Fractal structures formed by kinetic aggregation of aqueous gold colloids. *Phys. Rev. Lett.*, Vol. 52, pp. 1433-1436

Wolthers, W.; van den Ende, D.; Bredveld, V.; Duits, M. H. G.; Potanin, A. A.; Wientjens, R. H. W.; Mellema, J. (1997). Linear viscoelastic behavior of aggregated colloidal dispersions. *Phys. Rev. E*, Vol. 56, pp. 5726-5733

Zhang, Q.; Archer, L. A. (2002). Poly(ethylene oxide)/silica nanocomposites: structure and rheology. *Langmuir*, Vol. 18, No. 26, pp. 10435-10442

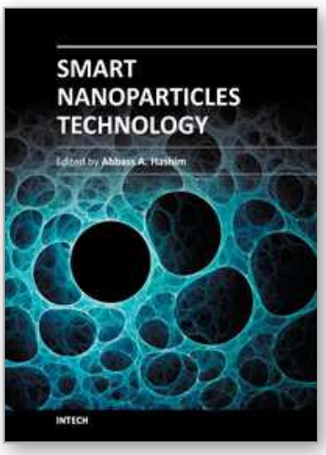

Smart Nanoparticles Technology

Edited by Dr. Abbass Hashim

ISBN 978-953-51-0500-8
Hard cover, 576 pages
Publisher InTech
Published online 18, April, 2012
Published in print edition April, 2012

In the last few years, Nanoparticles and their applications dramatically diverted science in the direction of brand new philosophy. The properties of many conventional materials changed when formed from nanoparticles. Nanoparticles have a greater surface area per weight than larger particles which causes them to be more reactive and effective than other molecules. In this book, we (InTech publisher, editor and authors) have invested a lot of effort to include 25 most advanced technology chapters. The book is organised into three well-heeled parts. We would like to invite all Nanotechnology scientists to read and share the knowledge and contents of this book.

How to reference

In order to correctly reference this scholarly work, feel free to copy and paste the following:

Giovanni Filippone and Domenico Acierno (2012). Nanoparticle Dynamics in Polymer Melts, Smart Nanoparticles Technology, Dr. Abbass Hashim (Ed.), ISBN: 978-953-51-0500-8, InTech, Available from: http://www.intechopen.com/books/smart-nanoparticles-technology/dynamics-of-nanoparticles-in-polymer-melts

INTECH
open science | open minds

InTech Europe
University Campus STeP Ri
Slavka Krautzeka 83/A
51000 Rijeka, Croatia
Phone: +385 (51) 770 447
Fax: +385 (51) 686 166
www.intechopen.com

InTech China
Unit 405, Office Block, Hotel Equatorial Shanghai
No.65, Yan An Road (West), Shanghai, 200040, China
中国上海市延安西路65号上海国际贵都大饭店办公楼405单元
Phone: +86-21-62489820
Fax: +86-21-62489821

IntechOpen